Characterisation of macro-porous silicon for electronic applications

T.S. Perova*[a], E.V.Astrova**[b], R. Maurice[a], D. Potapova[a], T.N. Vasunkina[b], and R.A. Moore[a]

[1]Department of Electronic & Electrical Engineering, Trinity College, Dublin 2, Ireland, [2]Ioffe Physical-Technical Institute, St.-Petersburg, Russia

ABSTRACT

Micro-Raman spectroscopy was used in this study for the analysis of the influence of process conditions on the strain and stress in macro-porous layers. As expected, it was found that oxidation results in significant wafer bending, depending on the layer porosity. The magnitude of stress of about 0.33 GPa was found for ma-PS sample with lattice constant of 4 μm while for sample with the lattice constant of 12 μm it was only 0.175 GPa. Dissolution of the oxide layer restores the flatness of the samples after the first oxidation. Repetition of the oxidation cycles leads to a "memory effect", as the residual deformation increases. The results are consistent with results obtained for similar samples using X-ray diffractometry and topography and curvature measurements.

1. INTRODUCTION

Macro-porous silicon (*ma*-PS) is a material with a system of regular cylindrical pores including reach-through pores and pores with depths ranging from a few microns up to hundreds of microns [1]. This material differs from micro-porous and meso-porous silicon, not only by the pore diameter, but also by the high periodicity of the structure. The pore diameter lies in the range ~ 1-50 μm for *ma*-PS while in the case of micro-porous silicon the diameter is in the range 0.002-0.03 μm and for meso-porous silicon it ranges from about 0.01 - 1 μm. The electrical properties of macro-porous silicon (*ma*-PS) are close to those of bulk silicon. The crystalline lattice of macro-porous Si, contrary to micro-porous Si, is not disturbed, which permits its use in the active region of devices. For example as was shown in Ref. [2] the diffusion of boron and phosphorus impurities into *ma*-PS walls enables the formation of junctions of ~150-250 μm depth. *ma*-PS was quasi-uniformly doped and the doped layer had a flat diffusion front in the monocrystalline part. n-n^+ structure formed this way can replace conventional epitaxial techniques. Using these technique a diode with a thin base of 20 mm in diameter (Fig.1) has been fabricated.

Any potential application requires that the proposed structure will be compatible with standard Si processing. Stress and strain usually accompany the manufacturing process of devices from macro-porous Si due to the difference in thermal expansion coefficient for Si and silicon oxides. This leads to a permanent deformation in structures

*perovat@tcd.ie; phone 353 1 608-3802; fax 353 1 677-2442; http://www.tcd.ie; Department of Electronic & Electrical Engineering, University of Dublin, Trinity College, Dublin 2, Ireland; **east@pop.ioffe.rssi.ru; phone. 7812 247 99 57; fax 7812 247 91 23; http://www.ioffe.rssi.ru/ Ioffe Physical Technical Institute, Polytekhnicheskaya 26, 194021 St.Petersburg, Russia

Opto-Ireland 2002: Optics and Photonics Technologies and Applications, Thomas J. Glynn, Editor, Proceedings of SPIE Vol. 4876 (2003) © 2003 SPIE · 0277-786X/03/$15.00

Downloaded from SPIE Digital Library on 02 Feb 2010 to 134.226.1.229. Terms of Use: http://spiedl.org/terms

containing macro-porous Si. Recently a number of X-ray diffraction and topography investigations have been performed on the analysis of the crystalline lattice deformations during macro-porous Si preparation [3-6]. It has been shown that strain in a macro-porous Si lattice depends on the specific area. It should be noted that this strain is not always harmful, but can be used to develop focusing systems for X-ray and neutron optics. However, X-ray diffraction methods do not give information on stress values and their distribution on a micro scale.

Micro-Raman spectroscopy has been applied in the past for the study of stress distribution in layered micro-porous silicon [7-9]. Quite substantial biaxial stress (~ 4- 9 kBar) was found for the layers with different porosities. Some work has been carried out to study stress in trench structures which can be considered somewhat similar to macro-porous silicon [10]. However to the best of our knowledge no investigations have been performed to analyse the stress in macro-porous silicon. This paper is devoted to the study of stress in a number of porous Si samples with different size and configuration of pore. Some of the results obtained are discussed in conjunction with X-ray diffraction data.

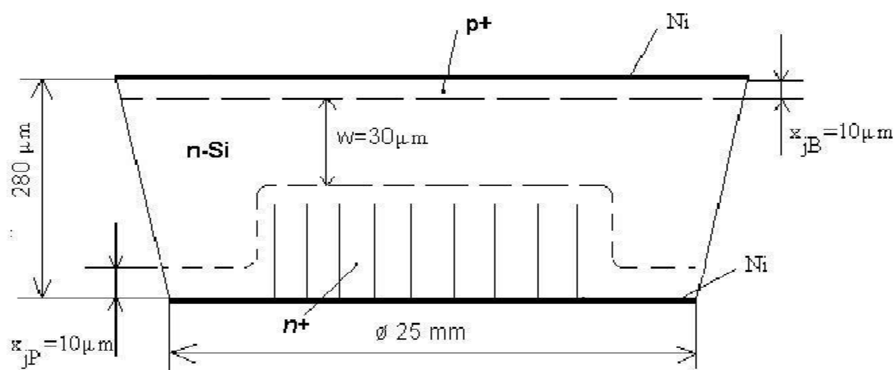

Figure 1. Diode with a thin base on macro-porous Si n-n$^+$substrate [2].

(100)

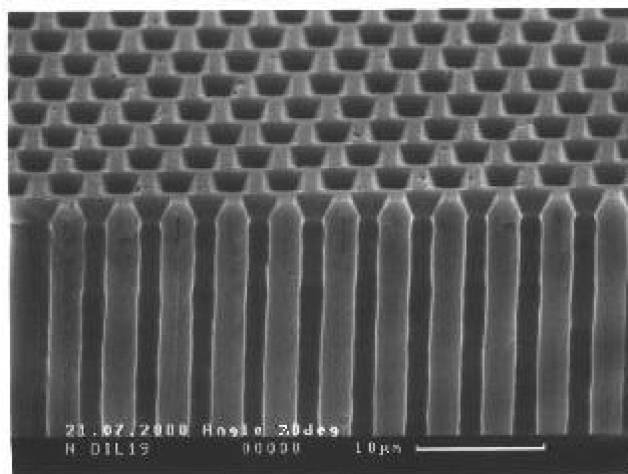

Figure 2. SEM image of macro-porous silicon with triangular "lattice" and period of 4 μm.

Downloaded from SPIE Digital Library on 02 Feb 2010 to 134.226.1.229. Terms of Use: http://spiedl.org/terms

2. EXPERIMENTAL

Sample preparation

The macroporous silicon used in this study (as shown in Fig. 2) has a system of regular cylindrical pores of micrometer scale diameter and high aspect ratio. The starting material was single crystal (100)-oriented Czochralski grown n-type silicon with a resistivity ρ=15 and 5Ω·cm. A standard photolithographic process was used to form pits spaced 12 μm (or 4 μm) apart on the polished surface of the silicon. Deep pores were etched electrochemically in 2.5% HF aqueous-ethanol solution for 300 to 450 min under backside illumination [1]. The voltage used was 5V and a constant current density of j=3 mA/cm^2 was used. The pore depth ranged from 150-250 μm up to the reach-through pores. The pore diameter was around d=2-4 μm which corresponds in the case of the triangular lattice to a porosity of ~ 2.5% (for 12 μm lattice) and to 22.5% (for 4 μm lattice).

The pores with depth of 150-250 μm were etched from predefined pits in the central part of the wafer's face side. On the wafer face, seeding pits formed a regular macropore pattern: either a triangular lattice with 12 μm period (photomask AT-3), or a honeycomb structure with pores in the apexes of a regular hexagon with a side of 12 μm and additional pores in the center of each side (photomask AT-2). The density of macropores was $N = 7.94 \cdot 10^5$ and $1.33 \cdot 10^5$ cm^{-2} for AT-3 and AT-2 masks, respectively; this yields different porosity of *ma*-Si for the same pores diameter. To obtain the reach through channels the back side of the wafers were mechanically polished. For some experiments the *ma*-PS with removed pit layer or removed nonporous edge have been used.

A number of different *ma*-PS samples have been used to study stress distribution across the wafer by means of micro-Raman spectroscopy. These samples are: i) as prepared ma-PS samples with triangular "lattice" periods of 4 and 12 μm (Fig. 2 and 3a) and a "honeycomb-like" lattice (Fig. 3b) and ii) oxidised ma-PS samples. The SiO_2 layer in both cases was 1.2 μm thick. The distribution of stress in some of these samples was also studied during the cycle of consecutive oxidation and oxide removal in HF solution.

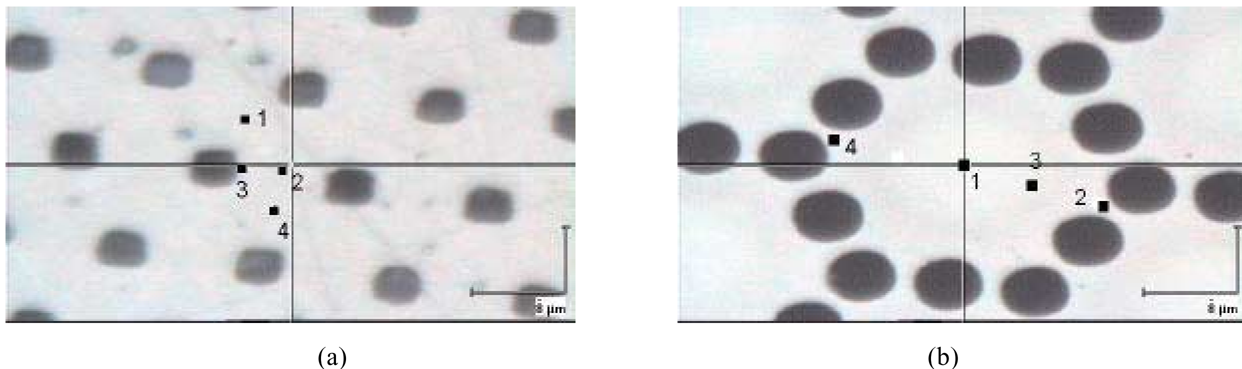

(a) (b)

Figure 3. Ma-PS samples with triangular lattice (a) and honeycomb-like lattice (b) used for investigations. The numbers indicate the points on the sample from which single Raman spectrum was collected.

Raman measurements

Micro-Raman measurements were performed in backscattering mode on a Renishaw Raman microscope system 1000. The 514.5 nm line of an Ar^+ ion laser at a power of 3 mW was used as the excitation source. The light was focused onto the sample using a Leica optical microscope with the size of the laser spot less than 1 μm. A Peltier cooled CCD detector with 1 cm^{-1} resolution was used to analyse the spectrum. Line-mapping experiments have been

Downloaded from SPIE Digital Library on 02 Feb 2010 to 134.226.1.229. Terms of Use: http://spiedl.org/terms

performed when the distribution of stress along a certain direction on the sample is required. The sample is placed underneath the objective lens on an XYZ transportation stage, which allows measurements with the sample moving with a minimum step of 0.1 μm.

3. RESULTS AND DISCUSSIONS

The crystalline silicon Raman spectrum in a phonon region mainly consists of a narrow peak around 520 cm^{-1} with a width of about 3.5 cm^{-1}. The spectrum arises from scattering by long-wavelength transverse optical phonons [10]. With a state–of-the-art spectrometer it is possible to identify a shift in the Raman band of the order of ~0.01 cm^{-1} [10]. Background baseline removal followed by a line fit using a Lorentzian function allows three components of the Raman spectrum to be determined viz. intensity, half width and position. These variations are related to the composition, defect density, and magnitude of stress respectively. A relationship exists between the stress, σ (in Pa), and the Raman shift, $\Delta\omega$ (in cm^{-1}) [10]:

$$\Delta\omega = -2\times10^{-9}\sigma \,, \tag{1}$$

where $\Delta\omega = (\omega_{stress} - \omega_{ref})$ (in cm^{-1}), ω_{stress} is the peak frequency of the phonon band of silicon under the stress and ω_{ref} is the peak frequency of the phonon band of the stress-free silicon wafer. A positive or negative shift in the Raman peak position corresponds to compressive or tensile stress, respectively [10], assuming uniaxial stress only i.e within the plane of the wafer.

The single plane Raman measurements at different positions on non-oxidized samples with various "lattice" structures show that stress increases for samples with high porosity and is higher in between the pores. This was also confirmed by line mapping Raman experiment shown in Fig. 4 for honeycomb-like structure. The stress is also different from the front and from the backside of the wafer depending on the size of the specific area (see [5,6] for details). For example for one of the sample with reach-through pores the stress from the front side (with pits) was approximately 1.3 times biger than from the back side. This is because the area occupied by pores (so called specific area) is larger from the front side due to the pits size.

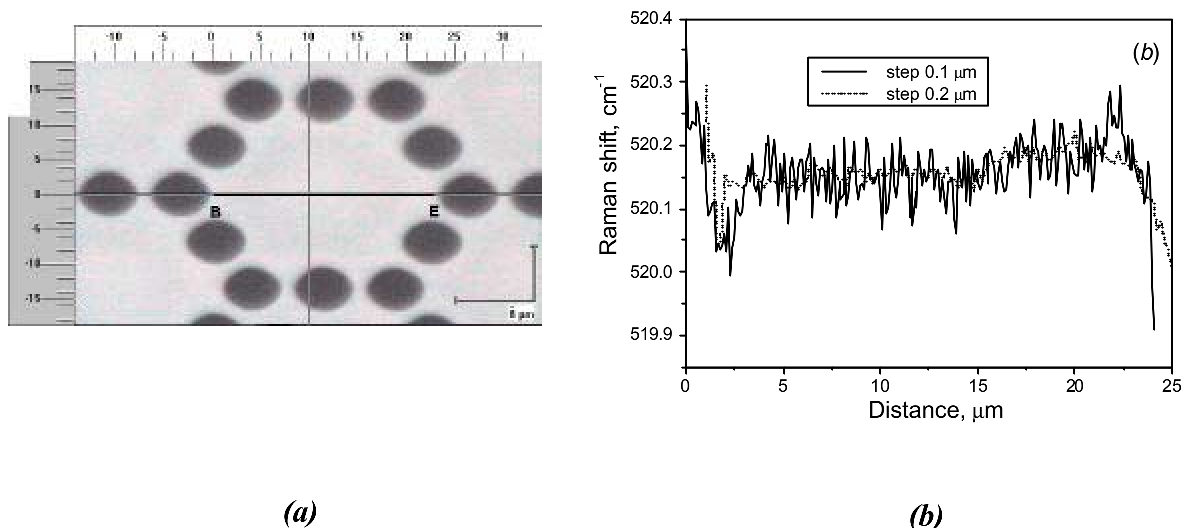

Figure 4. Raman line-mapping experiment (b) performed for the as prepared *ma*-PS sample with honeycomb-like structure as it shown in (a). The measurements performed along the central horizontal line indicated in fig.3a.

Downloaded from SPIE Digital Library on 02 Feb 2010 to 134.226.1.229. Terms of Use: http://spiedl.org/terms

After oxidation the single Raman measurements were performed on the sample with reach through pores (and removed pits) at different positions, starting from the point near the centre of the porous part, which corresponds to x=0 in Fig. 5a, to the edge of the sample (corresponding to x=10 mm). To reveal stress distribution near the boundary between the central porous part and nonporous edge of the wafer, the line mapping Raman measurements with a step size of 300 μm were also performed for this sample from x=6 mm up to x=10 mm. It should be noted that Raman measurements were performed from the bottom part of the sample. Figs. *5b* and 5*c* show that the stress is tensile at the middle of the porous part and compressive at the concave edge. The magnitude of stress varies from approximately -0.066 GPa to + 0.085 GPa. These results are in accordance with X-ray diffraction data obtained for the same sample in Refs. [5,6].

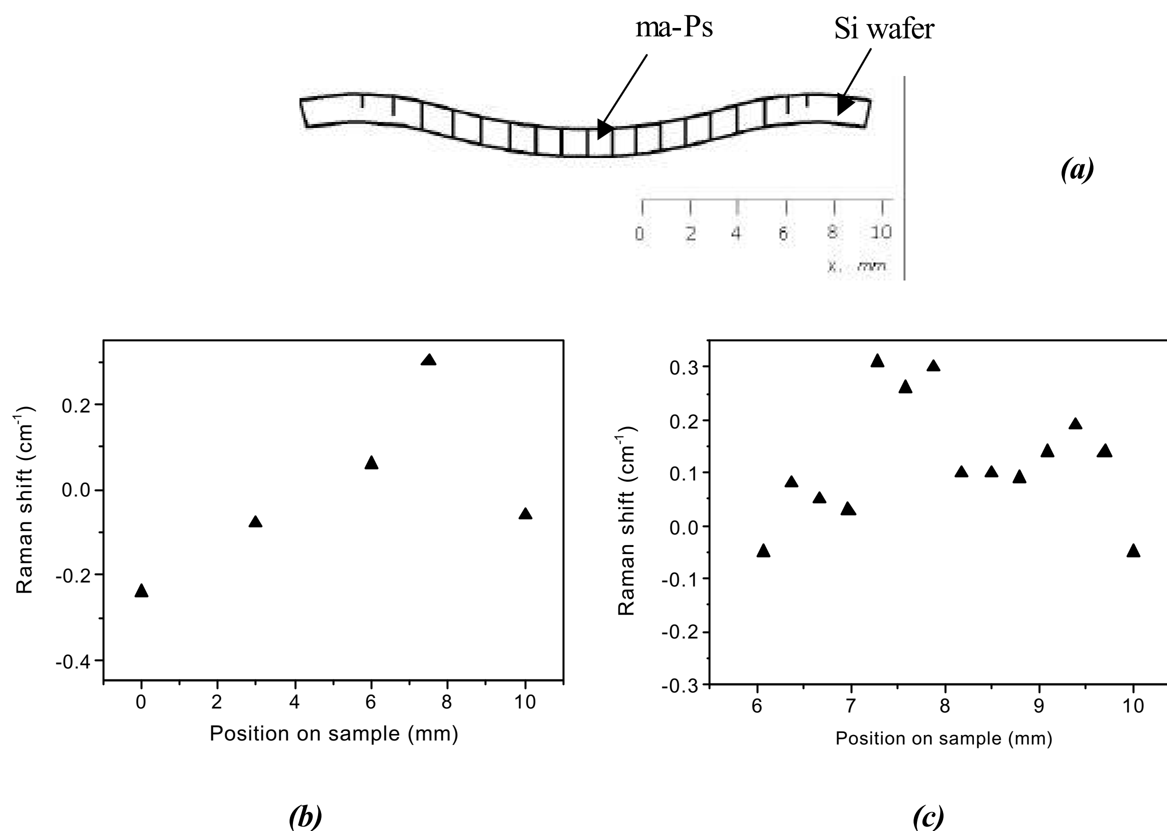

Figure 5. Shape of oxidized ma-Ps sample with trough channels spaced in 12 μm (triangular lattice) (a), dependence of the Raman shift along its diameter (b) and near nonporous edge (c).

As was shown in Refs. [5,6], the radius of curvature R and its sign after oxidation depends on the sample structure. The face surface of the oxidized *ma*-PS with both reach through and non-through pores with pits is convex (Fig.6a), while the face surface of samples with reach-through pores without pits is concave (Fig. 5a). Both kinds of the samples were investigated in this work. Moreover, sample shown in Fig. 6a has higher porosity p=~22.5% which results in a lower radius of curvature after the oxidation. Raman measurements performed for these two samples also show quite strong dependence of stress on porosity. In particular, for sample with lattice constant of 4 μm the magnitude of stress around 0.33 GPa was obtained after the first step of oxidation, while for similar sample with lattice constant 12 μm the stress magnitude was only 0.175 GPa.

Downloaded from SPIE Digital Library on 02 Feb 2010 to 134.226.1.229. Terms of Use: http://spiedl.org/terms

The results of line-mapping measurements (Raman shift and stress) for the sample shown in Fig.6a, after the first oxidation, are shown in Fig. 6b. As can be seen from this figure the stress on this bowed wafer changes from tensile with a magnitude of ~ 0.33 Gpa at the centre of the wafer (on the convex part) to compressive with a magnitude of ~ -0.14 GPa at the edge. These data agree with the results obtained from measurements on bowed microporous Si wafers [11]. The investigation of the stress behavior for the *ma*-PS sample with lattice constant of 12 μm and with pits and edges has been performed during the oxidation-dissolution cycle. Fig. 7 demonstrates the results of these investigations. Here the maximum stress observed after the first oxidation process was 0.175 GPa. After removal of the oxide the stress decreases substantially (by approximately of two orders of magnitude) and becomes nearly equal to the stress in the as-received *ma*-PS sample. After the second and the third step of the oxidation-dissolution cycle the stress in the oxidized wafer increases linearly with the pore diameter and it does not reduce to the initial value (in as-prepared porous sample) after the oxide removal.

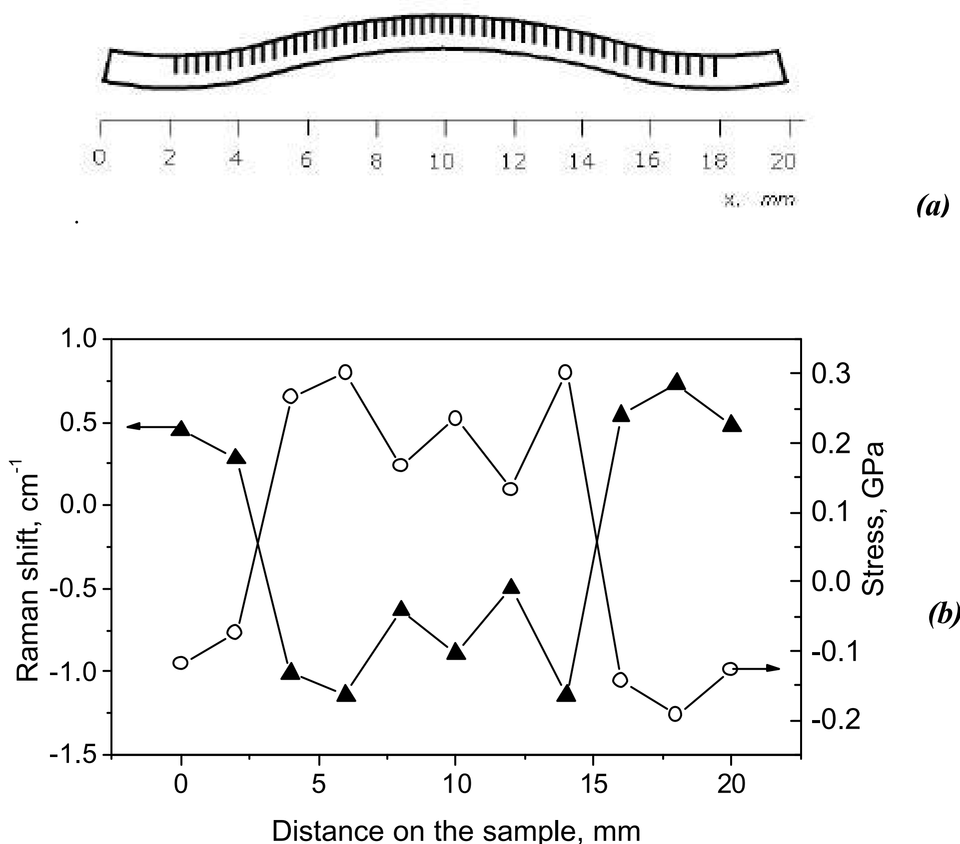

Figure 6. Shape of oxidized sample with dead-end channels spaced in 4 μm (triangular lattice) - (a) and the relative Raman shift and the calculated stress for this sample (b). Lines joining the data points are there to assist visual perception

Downloaded from SPIE Digital Library on 02 Feb 2010 to 134.226.1.229. Terms of Use: http://spiedl.org/terms

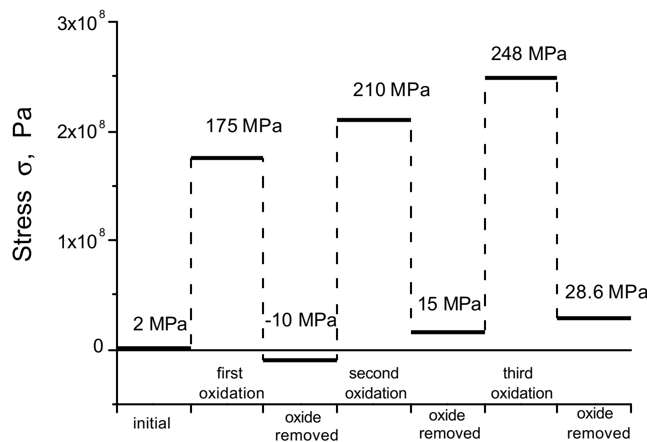

Figure 7. Stress obtained for *ma*-PS sample with edges and pits during the oxidation-dissolution cycle using micro-Raman spectroscopy.

Stress after the third step of oxide removal remains at a magnitude of ~ 0.0286 GPa, which means that the lattice becomes deformed after a few steps of oxidation and oxide removal. Thus each subsequent oxidation-dissolution cycle increases the strain in the oxidized state and the residual strain after SiO_2 removing, demonstrating the "memory" effect. These results are in accordance with X-ray diffraction and method of curvature measurements presented in papers [5,6]. The main reason of *ma*-PS deformation is the oxidation of the pores walls. The oxide introduces stress due to the difference in the thermal expansion coefficient of Si and SiO_2. The strain has a mixed elastic-plastic character.

ACKNOWLEGMENTS

Higher Education Authority (HEA) Ireland, Russian Fund of Basic Research and European Community are gratefully acknowledged for providing financial support towards this work through HEA Grant for Advanced Materials, Scientific School Support Program (Grant N 00-15-96770) and INTAS 01-0642.

REFERENCES

1. V. Lehmann, "Electrochemistry of Silicon", Wiley-VCH, Verlag GmbH, Weinheim, 2002.
2. E.V. Astrova, I.V. Grekhov, A.V. Nashchekin, V.V. Ratnikov, A.D. Remenyuk, I.L. Shulpina, A.G. "Tkachenko, and V.B. Voronkov, "Deep diffusion doping of macroporous silicon", Phys.Stat.Sol. (a), **182**, p.p. 145-150, 2000.
3. Astrova EV, Ratnikov VV, Remenyuk AD, Tkachenko AG, and Shul'pina IL, "Nondestructive Diagnostics of Microchannel (Macroporous) Silicon by X-ray Topography", Technical Physics Letters **26**, pp.1087-1090, 2000 (Translated from Pis'ma v JETP **26,** 31, 2000).
4. Astrova EV, Remenyuk AD, Tkachenko AG, and Shul'pina IL, "Real Structure of a Microchannel Silicon Studied by X-ray Diffraction", Technical Physics Letters, **27**, pp. 41-44, 2001. (Translated from Rus. Pis'ma v JETP, **27**, 1 , 2001).

Downloaded from SPIE Digital Library on 02 Feb 2010 to 134.226.1.229. Terms of Use: http://spiedl.org/terms

5. Astrova EV, Ratnikov VV, Remenyuk AD, and Shul'pina IL, "Strains and Crystal Lattice Defects Arising in Macroporous Silicon under Oxidation", Semiconductors, **36,** p.p.1033-1042**,** 2002
6. Astrova EV, Ratnikov VV, Remenyuk AD, and Shul'pina IL, "Strains in macroporous silicon introduced by cyclic oxidation ", Phys.Stat.Sol. A, 2002 (in press).
7. S. Manotas, F. Agullo-Rueda, J.D. Moreno, R.J. Martin-Palma, R. Guerrero-Lemus and J.M. Martinez-Duart, "Depth-resolved microspectroscopy of porous silicon multilyers", *Appl.Phys.Lett*. **75**, pp. 977-979, 1999.
8. F. Agullo-Rueda, J.D. Moreno, E. Montoya, R. Guerrero-Lemus and J.M. Martinez-Duart,"Influence of wavelength on the Raman line shape in porous silicon", *J.Appl.Phys***. 84**, pp. 2349-2351, 1998.
9. M. Yang, D. Huang, P. Hao, F. Zhang, and X. Wang, "Study of the Raman peak shift and the linewidth of light-emitting porous silicon", *J.Appl.Phys.* **75**, pp. 651-653, 1994.
10. I. De Wolf, "Micro-Raman spectroscopy to study local mechanical stress in silicon integrated circuits," *Semicond. Sci.Technol.* **11**, pp. 139-154, 1996.
11. K. Barla, R. Herino, G. Bomchil, "Stress in oxidized porous silicon layers", *J.Appl.Phys.* **59***,* pp.439-41, 1986.

Downloaded from SPIE Digital Library on 02 Feb 2010 to 134.226.1.229. Terms of Use: http://spiedl.org/terms